CHEMISTRY OF MATERIALS
Cite This: Chem. Mater. 2019, 31, 1250−1257
Article
pubs.acs.org/cm

Area-Selective Atomic Layer Deposition of ZnO by Area Activation Using Electron Beam-Induced Deposition

Alfredo Mameli,[†] Bora Karasulu,[†,‡] Marcel A. Verheijen,[†] Beatriz Barcones,[†,§] Bart Macco,[†] Adriaan J. M. Mackus,[†] Wilhelmus M. M. Erwin Kessels,[†] and Fred Roozeboom*[,†,∥]

[†]Department of Applied Physics, Eindhoven University of Technology, P.O. Box 513, 5600 MB Eindhoven, The Netherlands
[‡]Department of Physics, Cavendish Laboratory, University of Cambridge, 19, J. J. Thomson Avenue, CB3 0HE Cambridge, U.K.
[§]NanoLab@TUe, 5600 MB Eindhoven, The Netherlands
[∥]TNO-Holst Centre, High Tech Campus 21, 5656 AE Eindhoven, The Netherlands

Supporting Information

ABSTRACT: Area-selective atomic layer deposition (ALD) of ZnO was achieved on SiO_2 seed layer patterns on H-terminated silicon substrates, using diethylzinc (DEZ) as the zinc precursor and H_2O as the coreactant. The selectivity of the ALD process was studied using in situ spectroscopic ellipsometry and scanning electron microscopy, revealing improved selectivity for increasing deposition temperatures from 100 to 300 °C. The selectivity was also investigated using transmission electron microscopy and energy-dispersive X-ray spectroscopy. Density functional theory (DFT) calculations were performed to corroborate the experimental results obtained and to provide an atomic-level understanding of the underlying surface chemistry. A kinetically hindered proton transfer reaction from the H-terminated Si was conceived to underpin the selectivity exhibited by the ALD process. By combining the experimental and DFT results, we suggest that the trend in selectivity with temperature may be due to a strong DEZ or H_2O physisorption on the H-terminated Si that hampers high selectivity at low deposition temperature. This work highlights the deposition temperature as an extra process parameter to improve the selectivity.

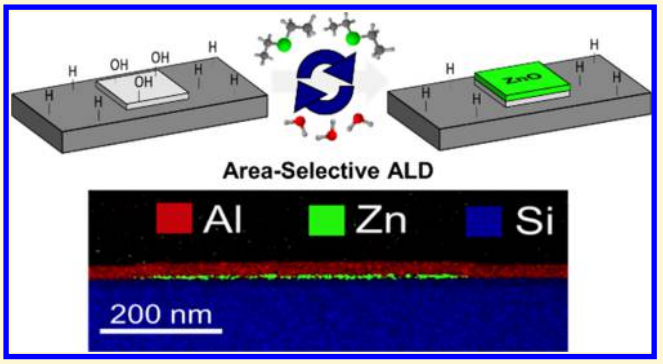

1. INTRODUCTION

The scaling in state-of-the-art device nanofabrication requires ever finer patterning steps with increasing demands on feature alignment. This scaling poses serious challenges as the features become smaller than what can be patterned with the conventional top-down fabrication.[1] Nanopatterning involving area-selective deposition, in particular area-selective atomic layer deposition (ALD), has been identified as a potential solution to aid nanoscale device manufacturing.[1−4]

ALD relies on the self-limiting surface reactions that take place between surface functional groups and vapor-phase precursors. The chemospecific nature of the technique allows precise control of the location, where these reactions take place by tailoring the surface chemistry. From a patterning point of view, two main approaches for achieving area-selective ALD can be distinguished:

(1) area deactivation, in which a part of the surface is rendered inert toward the ALD process chemistry;[5] and

(2) area activation, where conversely, an inert surface is locally activated to enable a specific ALD chemistry.[6,7]

When no subtractive steps are employed, the latter approach is referred to as direct-write ALD.[4,7−9] This specifically combines patterning and ALD into a bottom-up (i.e., additive) approach.

Recently, we have demonstrated an area-selective ALD approach for In_2O_3:H with micrometer-scale pattern dimensions, consisting of area activation using a μ-plasma printer, followed by thermal ALD of In_2O_3:H.[9] This approach relies on the long nucleation delay observed for In_2O_3:H ALD on H- and NH_x-terminated silicon substrate surfaces, when using an indium cyclopentadienyl (InCp) precursor and a combination of H_2O and O_2 as coreactants. Conversely, deposition takes place almost directly on OH-terminated silicon surfaces.[10] High selectivity was demonstrated for this process, and the material properties were shown to be similar to those of the In_2O_3:H deposited on blanket silicon substrates. The high selectivity could be attributed to the thermodynamically unfavorable chemisorption of the precursor, InCp, on the H-terminated surfaces.

Here, we extend the approach to another metal oxide, that is, ZnO, which can be considered as a model system for a class of

Received: July 25, 2018
Revised: January 28, 2019
Published: January 31, 2019

oxides that are technologically relevant for applications in sensing, optoelectronic, and memory devices.[11−14] ZnO was deposited using diethylzinc (DEZ) and H_2O. In contrast to the In_2O_3:H case,[9] here, the selectivity is attributed to the differences in precursor reaction kinetics on growth and nongrowth areas (NGA). Moreover, the effect of the deposition temperature has been experimentally investigated and discussed. Finally, the area-activation step has been performed at nanoscale dimensions which align well with the aforementioned search for new nanopatterning approaches. The combination of the activation step with the subsequent ALD building step is schematically illustrated in Figure 1. In the patterning step, an ultrathin SiO_2 seed layer is locally deposited using electron beam-induced deposition (EBID).[15] In this way, nanoscale OH-terminated regions are defined that are reactive toward the ZnO ALD chemistry, as opposed to the H-termination of the starting surface. In the building step, ZnO is grown on the activated area by alternating the two ALD half-reactions (pulses A and B) in a cyclic fashion.

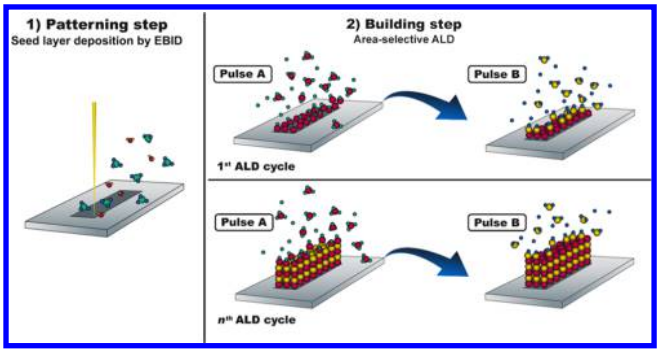

Figure 1. Schematic representation of the area-selective ALD approach of ZnO on an H-terminated amorphous Si layer. First, nanoscale patterns are defined by depositing a SiO_2 seed layer using EBID (patterning step 1). Next, ZnO is deposited selectively on the activated areas (i.e., SiO_2 seed layer patterns) by area-selective ALD (building step 2). This ALD process consists of cycles of two alternating half-reactions: precursor dosing in pulse A and coreactant dosing in pulse B.

Because of its ability to directly deposit nanostructures with sub-10 nm lateral dimensions without shape constraints, the EBID technique allows to meet some of the stringent requirements of modern and future device manufacturing in terms of resolution.[16,17] Furthermore, the EBID technique enables deposition of materials in a direct-write (i.e., no subtractive steps) fashion on various substrates, including polymers.[18] This unique capability makes it a suitable technique for high-resolution bottom-up patterning of areas consisting of different materials having specific chemical functionalities.

In this work, the key factors that impart selectivity to the ALD process for ZnO are discussed in terms of nucleation delay, as measured by in situ spectroscopic ellipsometry (SE). The selectivity is further elaborated on a molecular-scale level, as corroborated by density functional theory (DFT) calculations. Furthermore, the area-selective ALD was experimentally demonstrated using scanning electron microscopy (SEM) and for the most illustrative sample, using transmission electron microscopy (TEM) cross-sectional inspection combined with energy-dispersive X-ray (EDX) spectroscopy performed in the scanning TEM mode. The effect of the deposition temperature on the selectivity (to be defined in Section 3.2) between 100 and 250 °C is also studied through a combination of in situ SE and SEM. The selectivity is found to be higher at high deposition temperatures. A possible mechanism that may play a role in the selectivity loss at lower temperatures will be discussed.

2. EXPERIMENTAL SECTION

2.1. Substrate Preparation Method. Ten nanometers-thick a-Si/H films were deposited on p-type c-Si(100) coupons with native oxide, using inductively coupled plasma chemical vapor deposition (ICP-CVD) from SiH_4 and Ar at 50 °C.

2.2. Patterning Step. After deposition of the a-Si/H starting surfaces, the samples were quickly transferred to the SEM system. Here, localized activation was achieved by depositing an ultrathin seed layer of SiO_2 using EBID. The sample was kept at room temperature. The nanoscale patterns were generated in an FEI Nova 600 NanoLab DualBeam SEM system. Tetraethyl orthosilicate (TEOS) was used as the Si-precursor, together with H_2O to generate SiO_2 (with ∼26 at. % C impurities) patterns. Both gases were simultaneously introduced into the SEM chamber through a gas injection system at a pressure of 2.5×10^{-5} mbar. The SiO_2 nanoscale patterns were generated by scanning an electron beam with 2, 5, 10, 15, or 30 kV acceleration voltages and currents between ∼0.04 and ∼0.14 nA. The volume per dose (i.e., the yield of SiO_2 EBID) was calculated for both 5 and 30 kV by depositing test structures and by determining their volume using SEM.

The calculated values were used to select settings for deposition of SiO_2 seed layers as thin as ∼1 nm for all of the accelerating voltages described above. The best spatial resolution of the seed layer was obtained for an acceleration voltage of 15 kV and a current of 0.14 nA. These settings were therefore used in this work. Right after the patterning step, the samples were transferred to the ALD reactor. The transfer was done within a few minutes in order to minimize possible oxidation and degradation of the H-termination of nontreated surface of the substrate because of the exposure to the ambient atmosphere.

2.3. ALD Process. For this study, a commercial ALD reactor (OPAL, Oxford Instruments) was used for depositing ZnO. DEZ [$Zn(C_2H_5)_2$] was employed as the zinc precursor and H_2O as the coreactant. A standard recipe was employed, for which the details can be found elsewhere.[19] The patterned ZnO samples described in this study were prepared using 80 ALD cycles at temperatures ranging from 100 to 250 °C (for completeness, the ZnO growth rate as a function of the deposition temperature is reported in the Supporting Information, Figure S1). The chamber pressure during the ALD process was ∼170 mTorr during the 50 ms DEZ pulses (A) and the Ar purges, with a spike of 250 mTorr during the 100 ms H_2O pulses (B).

2.4. Analytical Methods. Nucleation studies were carried out using in situ SE, performed with a J.A. Woollam M2000D ellipsometer. Morphology and surface coverage analyses of the ZnO structures prepared by area-selective ALD were carried out in an FEI Nova 600 Nanolab DualBeam SEM system using 10 kV and 0.54 nA. The same SEM system was used to prepare a cross-sectional lamella by means of focused ion beam milling. Before the lamella preparation, a protective layer of Al_2O_3 was deposited by thermal ALD using trimethylaluminum [TMA, $Al(CH_3)_3$] and H_2O as the precursor and coreactant, respectively. Cross-sectional TEM studies were performed in high-angle annular dark-field (HAADF) scanning mode STEM and in bright-field TEM modes using a probe-corrected TEM system (JEOL JEM ARM 200F) equipped with a 100 mm^2 Centurio SDD EDX spectroscopy detector for chemical analysis. TEM studies were employed to assess the selectivity of the process.[20−22]

2.5. DFT Methods. All electronic structure calculations were performed using the projector-augmented wave function[23,24] as implemented in the Vienna Ab initio Simulation Package, VASP v.5.3.5.[25−27] First-principles calculations were carried out using the generalized gradient approximation to the DFT.[28,29] The Perdew−Burke−Ernzerhof (PBE)[30] exchange correlation functional was employed with the Van der Waals interactions included on an empirical basis (PBE-D3).[31] Hydroxylated α-SiO_2 clusters were used as approximations of the EBID SiO_2 seed layers and c-Si with native oxide utilized in the experiments. Accordingly, H-terminated c-Si clusters were employed as approximations of the a-Si/H used in the

DOI: 10.1021/acs.chemmater.8b03165
Chem. Mater. 2019, 31, 1250−1257

experiments.[9] These simulation models of α-SiO_2 and H-terminated c-Si surfaces have been utilized for studying the precursor adsorption step in similar ALD processes.[9,10,32] Minimum energy pathways for the chemisorption of a DEZ precursor molecule on each surface were computed using the climbing-image nudge elastic band method,[33] as implemented in VASP-VTST tools.[34] The same method was used to study the chemisorption of an H_2O molecule on an H-terminated c-Si surface. Further details on model preparations and computations can be found in our previous reports.[9,10] Binding energies of DEZ or H_2O on various silicon surfaces through physisorption or chemisorption ($\Delta E_{p/c}$) were evaluated using eq 1.

$$\Delta E_{p/c} = E_{PS} - E_P - E_S \quad (1)$$

where E_{PS} is the total energy of the physisorbed/chemisorbed substrate−precursor complex and E_P and E_S are the total energies of an isolated DEZ (or H_2O) molecule and a given substrate surface, respectively. Here, physisorption can be described as the weak physical (noncovalent) binding of the DEZ (or H_2O) molecule on a given surface, whereas the chemisorption requires the chemical (covalent) bonding of the precursor (or the coreactant), accompanied by the loss of one of the ligands.

Gibbs free-energy changes ($\Delta G = \Delta(E_{elec} + E_{ZPE}) - T\Delta S$) associated with DEZ adsorption were estimated in the ideal gas limit at the typical ALD conditions (T = 50−400 °C and p = 100 mTorr), accounting for the translational, rotational, and vibrational contributions to the enthalpy and entropy terms (see the effect of temperature on the reaction energetics in the Supporting Information). All-atom vibrational analyses were performed using the dynamical matrix method (based on finite differences) implemented in VTST tools.[34]

3. RESULTS AND DISCUSSION

3.1. ALD of ZnO: Nucleation on SiO_2 and a-Si/H. Figure 2 shows the ZnO film thickness as a function of the number of ALD cycles, as measured by in situ SE, for a deposition temperature of 100 °C. The nucleation behavior was measured on a freshly deposited ∼10 nm a-Si/H film and on c-Si coupons with native oxide (hereinafter referred to as SiO_2), which can be considered as representative for the SiO_2 EBID seed layers. A relatively long nucleation delay of ∼80 cycles was observed on the a-Si/H substrate. After a transient regime,[35] linear growth starts with a growth per cycle (GPC) of ∼1.6 Å/cycle. In contrast, a very short nucleation delay is observed on SiO_2 before the film growth becomes linear with a GPC of ∼1.6 Å/cycle.

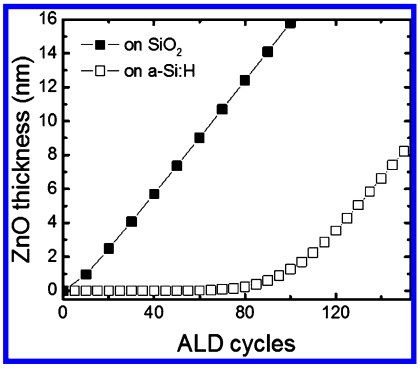

Figure 2. ZnO film thickness measured by in situ SE as a function of the number of ALD cycles performed on substrates with a native SiO_2 surface (closed squares) and with a ∼10 nm-thick a-Si/H layer (open squares). On SiO_2, the ZnO film thickness increases linearly after a short delay of a few cycles, whereas on a-Si/H, the ZnO deposition experiences a relatively long nucleation delay. Only after 80 ALD cycles, the growth also starts on the a-Si/H and enters a linear regime at about 120 cycles. Both depositions were carried out at 100 °C.

The results of Figure 2 represent a first indication that area-selective ALD of ZnO can be obtained by exploiting the difference in nucleation delays on the two surfaces. Furthermore, the nucleation curves suggest a selectivity window (expressed as the number of ALD cycles for which no deposition is obtained on the a-Si/H) of about 80 ALD cycles before deposition occurs on both surfaces and the selectivity is lost.

The key reason for the difference in nucleation delay lies in the surface chemistry because dissimilar surface groups have distinct kinetic barriers toward various thermodynamically favorable end states. Two reaction pathways were proposed to investigate the chemisorption of DEZ on the different surfaces from a theoretical point of view. Using DFT, activation and chemisorption energies were calculated for the following reactions

$$Si - H^* + Zn(C_2H_5)_2 \rightarrow Si - Zn - C_2H_5^* + C_2H_6 \quad (2a)$$

$$Si - OH^* + Zn(C_2H_5)_2 \rightarrow Si - O - ZnC_2H_5^* + C_2H_6 \quad (2b)$$

where the asterisks indicate the relevant surface groups.

DFT calculations indicate that the physisorption of DEZ on both surfaces is exothermic with similar energy gains (ΔE_p = −0.37 vs −0.34 eV, see the Supporting Information, Figure S2). Figure 3 shows the corresponding DFT-based energy profiles connecting the physisorbed and chemisorbed species given in reactions 2a and 2b. Both reactions are thermodynamically favored, with chemisorption energies of −0.98 and −1.25 eV. However, an activation energy of 1.16 eV was calculated for reaction 2a and 0.81 eV for reaction 2b. The difference in energy barriers points toward a kinetically hindered surface reaction in the case of DEZ on an H-terminated surface. This may explain the difference in nucleation delay observed in Figure 2. Assuming the pre-exponential factors in the Arrhenius equation to be similar in magnitude for the two reactions, at 100 °C, the difference in kinetic barrier translates into a rate constant 5.4 × 10^4 times higher on SiO_2 than on a-Si/H.

Because either DEZ or H_2O surface reactions can play a role in the loss of selectivity after a prolonged number of ALD cycles (as shown in Figure 2), the reaction energetics of the coreactant with the H-terminated c-Si was also investigated (see the Supporting Information, Figure S3). The H_2O exposure might cause uncontrolled surface activation through parasitic oxidation reactions of the a-Si/H. Figure S3 shows the corresponding DFT energy profile. The oxidation of H-terminated surface by H_2O was found to be a slower process (with an activation energy of 1.49 eV), as compared to the DEZ chemisorption (reaction 2a). These findings are in agreement with the well-known stability of H-terminated surfaces toward mild oxidants.[36−38] On the basis of these considerations and neglecting other possible effects that in reality may affect the deposition process (e.g., presence of multiple reaction pathways, surface defects, or impurities), the DFT results suggest that reaction 2a forms the limiting step eventually leading to selectivity loss and therefore to the nucleation of ZnO on a-Si/H.

3.2. Selectivity at 100 °C. To demonstrate the feasibility of the area-selective ALD method, ALD was performed to deposit ZnO on 500 × 500 nm^2 SiO_2 EBID patterns that were created on a ∼10 nm a-Si/H-coated substrate. Figure 4a,c shows 35 SiO_2

DOI: 10.1021/acs.chemmater.8b03165
Chem. Mater. 2019, 31, 1250−1257

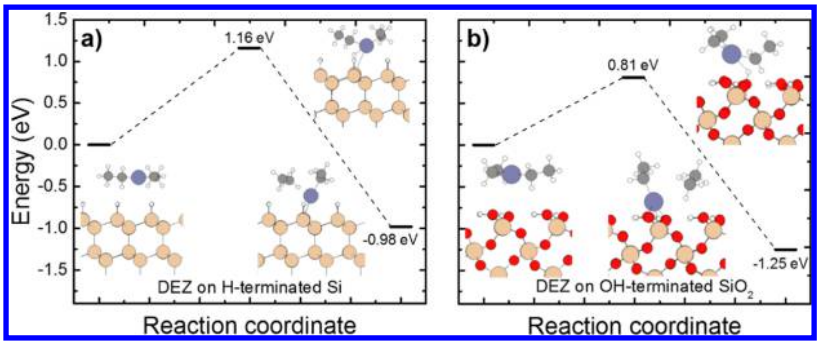

Figure 3. DFT/PBE-D3-level energy profiles for the chemisorption of DEZ on (a) H-terminated Si and (b) OH-terminated SiO_2. The zero corresponds to the physisorbed states: DEZ on H-terminated Si, $\Delta E_p = -0.37$ eV and on OH-terminated SiO_2 surface, $\Delta E_p = -0.34$ eV. Color code: light gray: carbon; light orange: silicon; red: oxygen; white: hydrogen; and blue: zinc.

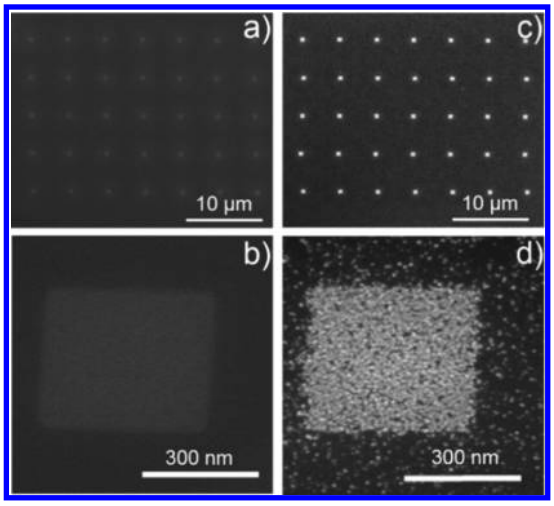

Figure 4. (a,b) Top-view SEM image of 35 EBID SiO_2 seed layers with an area of 500 × 500 nm^2 and a thickness of ∼1 nm. The high-magnification image in (b) shows a single pattern. (c,d) Top-view SEM image of a similar sample after 80 ALD cycles of ZnO, deposited at 100 °C. The high-magnification image in (d) shows a single pattern on which the polycrystalline ZnO is clearly visible.

EBID patterns before and after 80 ALD cycles of ZnO at a deposition temperature of 100 °C. ZnO deposition occurred predominantly on the SiO_2 EBID patterns, although some ZnO nucleation was observed outside the patterns, as will be discussed below.

The selectivity, S, was defined by Gladfelter in the field of area-selective CVD as[39]

$$S = \frac{N_{GA} - N_{NGA}}{N_{GA} + N_{NGA}} \qquad \text{with } 0 \le S \le 1 \tag{3}$$

Here, N_{GA} is the amount of material deposited (i.e., in terms of thickness, atomic areal density, coverage, etc.) on the surface on which growth should take place, referred to as the growth area (GA). N_{NGA} is the amount of material on the surface on which growth should be inhibited, referred to as the NGA. We note that area-normalized measurements should be considered when calculating the selectivity. By definition, $S = 1$ for perfectly selective processes and $S = 0$ for nonselective processes. When adopting this definition, S is dependent on the number of ALD cycles because deposition on the NGA can start after a nucleation delay.

Using the definition above, the selectivity of the ZnO ALD process was calculated using the thickness as measured by the SE data shown in Figure 2 and the coverage as imaged by the SEM in Figure 4d. After 80 ALD cycles of ZnO at a deposition temperature of 100 °C, the selectivity was measured to be 0.96 by SE and 0.83 by SEM. This difference in selectivity indicates that the SE data can overestimate the selectivity, which might be due to optical modeling as well as to the difficulties in modeling a noncontinuous film. Nevertheless, SE provides a good first indication of the selectivity and of its changes with the number of ALD cycles. These aspects will be elaborated more in detail below. Furthermore, it should be noted that the EBID-grown SiO_2 and the c-Si native oxide may also behave differently because of a high concentration of carbon impurities (∼26 at. %) that was measured for the SiO_2 deposited by EBID (see the Supporting Information, Figure S4).[40,41] Besides OH groups that will obviously be present on a SiO_2 surface, it has been suggested that electron irradiation of the TEOS ligands can lead to the formation of Si−C and Si−CH_3 and Si−H bonds.[42] The presence of these surface groups can inhibit DEZ adsorption, which can explain the slight difference in thickness and morphology that were observed between the ZnO deposited on EBID SiO_2 and native SiO_2. In addition, the thinner SiO_2 EBID patterns may also not form a completely closed film. Optimization of the EBID patterning step may further improve the process.

3.3. Effect of the Deposition Temperature on Selectivity. The temperature dependence of the selectivity was assessed by in situ SE measurements and further corroborated by SEM inspections. This dependence can provide additional insights into the mechanisms leading to selectivity loss after a certain number of ALD cycles. Figure 5a shows the evolution of the ZnO thickness as a function of the number of ALD cycles on blanket SiO_2 and a-Si/H samples for deposition temperatures of 100 and 250 °C. A larger nucleation delay is observed for deposition at 250 °C. Figure 5b shows the corresponding selectivity as a function of the number of ALD cycles, for 100 and 250 °C. The selectivity was calculated by combining the datasets shown in Figure 5a. For a deposition temperature of 100 °C, the selectivity decreases from 1.0 to 0.96 at 80 ALD cycles. By further increasing the number of cycles, the selectivity drops to 0.85 (at 100 cycles), which corresponds to a ZnO thickness of ∼1 nm on the NGA. For a deposition temperature of 250 °C, the selectivity, S, remains 1 until 110 cycles and then decreases to 0.95 at 140 ALD cycles.

These results clearly show an important aspect concerning the selectivity of this process: the selectivity window can be extended by increasing the deposition temperature but by staying below 350 °C. At a deposition temperature of 350 °C,

DOI: 10.1021/acs.chemmater.8b03165
Chem. Mater. 2019, 31, 1250−1257

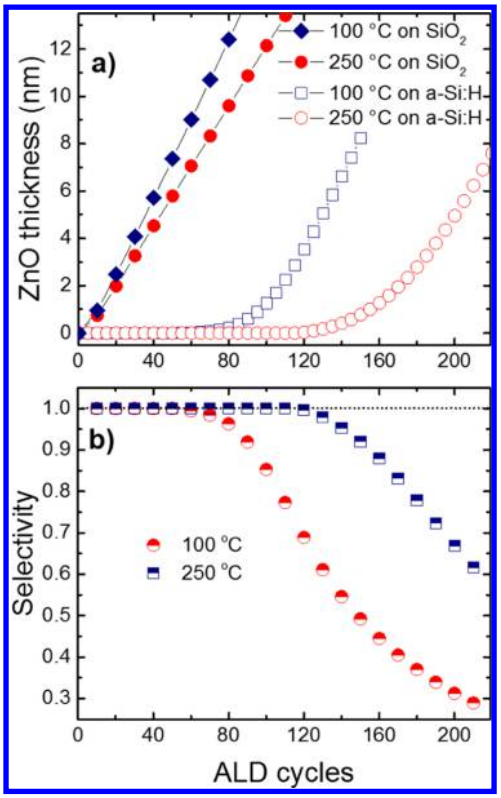

Figure 5. (a) ZnO nucleation curves on SiO_2 (closed symbols) and a-Si/H (open symbols) as measured by in situ SE for two different temperatures: 100 °C (square) and 250 °C (circle). (b) Selectivity as a function of the number of ALD cycles, for deposition temperatures of 100 °C (square) and 250 °C (circles). The horizontal dotted line at S = 1 indicates perfect selectivity.

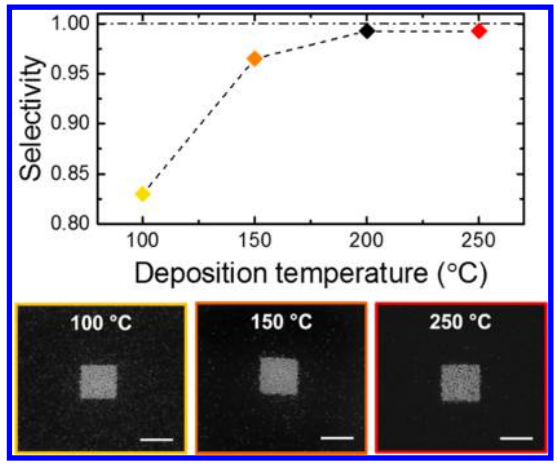

Figure 6. Selectivity for 80 ZnO ALD cycles as a function of the deposition temperature. The insets show the top-view SEM images of patterns realized using the same EBID parameters and number of ALD cycles, but different ZnO growth temperatures (100, 150, and 250 °C); scale bars are 500 nm. The horizontal dotted line at S = 1 indicates perfect selectivity.

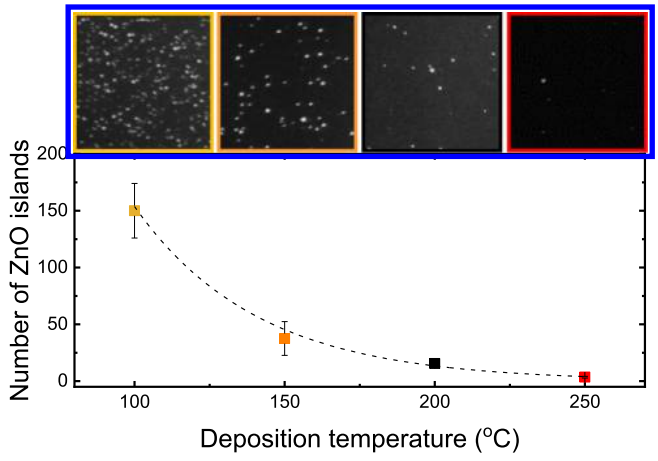

Figure 7. Statistical density of ZnO islands on the non-GA, after 80 ZnO ALD cycles for different deposition temperatures. The insets show color-coded top-view SEM images of the NGA (500 × 500 nm^2).

the selectivity is abruptly lost (see the Supporting Information, Figure S5). According to the idealized kinetic model described earlier using DFT calculations, one would expect the selectivity to increase with decreasing temperature because the chemisorption of DEZ on the H-terminated Si surface would be an even slower process. Indeed, the calculated Gibbs free energy for the final products and for the transition state (Figures S6 and S7) predicts larger selectivity at low temperature.

In contrast, the experimental results demonstrate that selectivity increases with the deposition temperature, thereby highlighting that several other factors (such as physisorption) may play a role in causing selectivity loss, as discussed below.

To further investigate the effect of the temperature, the selectivity was measured for different deposition temperatures between 100 and 250 °C, while keeping the number of ALD cycles fixed at 80. In this case, the selectivity was calculated using the ZnO surface coverage in and outside the patterned area, as measured by top-view SEM. Figure 6 shows the selectivity after 80 ALD cycles as a function of the deposition temperature, together with the SEM top-view images of the patterns deposited at 100, 150, and 250 °C as insets. The selectivity increases from 0.83 (at 100 °C) to 0.97 (at 150 °C) and 0.99 (at 200 and 250 °C). In other words, the SEM-measured selectivity data confirmed the results obtained using SE: the selectivity increases with the deposition temperature up to 250 °C. In order to explain the decrease in selectivity for low deposition temperature, a statistical analysis of the density of ZnO islands was conducted on several 500 × 500 nm^2 areas of the a-Si/H substrate. The data shown in Figure 7 reveal that, for the same number of cycles, the density of ZnO islands is one order of magnitude larger at 100 °C, compared to the one at 250 °C. The higher density of nucleation at 100 °C seems consistent with undesired reactions with physisorbed precursor or coreactant molecules on the NGA. Because the rate of desorption of physisorbed species decreases with decreasing the deposition temperature (for details see the Supporting Information, Figure S8), such physisorbed species may act as spurious nucleation sites and effectively decrease the selectivity of the process at low deposition temperatures.

A similar phenomenon has been observed for the ALD of Al_2O_3 on graphene: lower deposition temperatures resulted in higher Al_2O_3 coverage on a chemically inert graphene substrate.[43] Furthermore, Seo et al., using self-assembled monolayers (SAM) as NGA and titanium as the GA, argued that the selectivity for Al_2O_3 ALD is hampered because of the physisorption of TMA on the SAM.[44] The selectivity of their process could be increased by using lower partial pressures of precursor and by increasing the purge step in order to suppress this physisorption.

DOI: 10.1021/acs.chemmater.8b03165
Chem. Mater. 2019, 31, 1250−1257

Here, we suggest that a balance exists between the desorption rate of physisorbed species which may cause unwanted nucleation and the chemisorption rate on the NGA. Therefore, by tuning the deposition temperature, the rate of desorption and chemisorption can be altered and an optimum in selectivity was found between 250 and 300 °C, before the selectivity is completely lost at 350 °C. For a more detailed discussion and the complete set of nucleation curves from 100 to 350 °C, see the Supporting Information, Figure S5. Such an abrupt loss in selectivity is probably due to oxidation of the nongrowth surface or fast enough reaction kinetics with the DEZ. The DFT-calculated Gibbs free energies for the transition states suggest that the reason for the selectivity loss at 350 °C is indeed linked to the kinetics of the reactions because at about that temperature the two rates are equal. This observation strengthens further the idea that the selectivity of this specific process is under kinetic control.

3.4. Cross-Sectional TEM Analysis of Selectivity. Area-selective deposition was further investigated by cross-sectional TEM analysis of a pattern similar to those shown in the insets of Figure 6. Figure 8a shows an HAADF-STEM cross-sectional image of a ∼1 nm-thick SiO_2 EBID layer with a ∼7 nm-thick ZnO layer deposited by area-selective ALD using 80 ALD cycles at a deposition temperature of 250 °C. In Figure 8a,b, low-magnification images clearly show that ZnO deposition took place only on the activated area, that is, the SiO_2 seed layer. To further prove this, high-magnification images were taken from the central area of the pattern and from the region 250 nm away from this area (Figure 8c,d). Figure 8e,f presents the EDX elemental mappings of the pattern shown in the corresponding TEM images, which confirm the presence of Zn on the activated area. No Zn could be detected in the regions outside the SiO_2 EBID pattern, clearly demonstrating the selectivity of the ALD process.

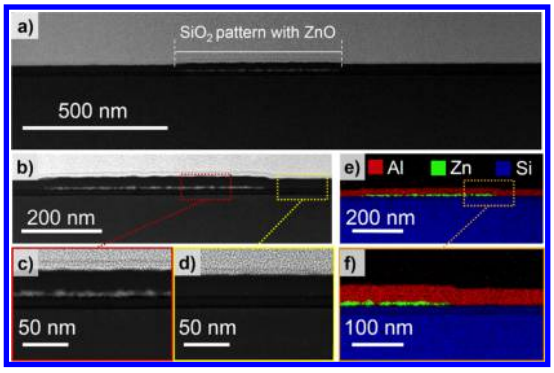

Figure 8. (a,b) Cross-sectional TEM images of a ZnO thin film that was selectively deposited (using 80 ALD cycles at 250 °C) on a ∼1 nm thick SiO_2 EBID pattern with a width of ∼500 nm. Low-magnification images show a pristine NGA outside the patterned GA, indicating that no ZnO deposition occurred on these surfaces. (c) High-magnification images showing the patterned GA and (d) region 250 nm away from the pattern, confirming the selectivity of the process. (e,f) EDX elemental mappings of the same pattern at two different magnifications also show the presence of ZnO on the SiO_2 GA and the absence of ZnO on the a-Si/H NGA.

4. CONCLUSIONS

We demonstrated a bottom-up patterning process at the nanoscale involving area-selective ALD of ZnO with a high selectivity on SiO_2 with respect to H-terminated Si. This process exploits the direct-write patterning capabilities of EBID to locally activate H-terminated surfaces by the deposition of SiO_2 seed layers.

Considering a defect-free H-terminated c-Si surface model, the energetics of the surface reactions were calculated by DFT methods. The results from DFT simulations suggest that the selectivity originates from a kinetically limited surface reaction between the DEZ precursor and an H-terminated Si surface, when compared to a similar reaction on an OH-terminated SiO_2 surface. Experimentally, we observed that increasing the deposition temperature plays a significant role in improving the selectivity of the process.

On the basis of these results, it can be inferred that at a fixed deposition temperature, the limiting step that causes selectivity loss is the DEZ precursor chemisorption on the H-terminated Si surface. We suggest that the low selectivity at low deposition temperature is due to strong physisorption of DEZ or H_2O that can contribute in hampering otherwise high selectivity through parasitic reactions. Our results indicate that several physico-chemical mechanisms (reaction kinetics, physisorption, etc.) can play opposite roles in determining the selectivity and detailed investigation of the surface chemistry at different temperatures is required to find the optimum deposition conditions for achieving high selectivity. Improving further the selectivity in area-selective ALD therefore remains a challenging problem and novel strategies to limit or counteract selectivity loss pathways are needed. We believe that the insights obtained in this work will expand the understanding of the mechanisms involved in area-selective ALD and in selectivity loss.

■ ASSOCIATED CONTENT

Supporting Information

The Supporting Information is available free of charge on the ACS Publications website at DOI: 10.1021/acs.chemmater.8b03165.

Growth per cycle for the thermal ALD of ZnO as a function of the substrate temperature; DFT/PBE-D3 level optimized geometries of the physisorbed DEZ on Si or SiO_2 surfaces; energy profiles computed by DFT method (PBE-D3) for the chemisorption of H_2O on H-terminated Si; energy-dispersive X-ray spectroscopy spectrum of a $1 \times 1 \times 0.5$ μm^3 SiO_2 EBID pattern; nucleation curves for the thermal ALD of ZnO; DFT-calculated Gibbs free energy of reaction for the DEZ chemisorptions; and estimated rate constant for DEZ adsorption on Si-H and desorption from Si-H surface (PDF)

■ AUTHOR INFORMATION

Corresponding Author

*E-mail: f.roozeboom@tue.nl.

ORCID

Alfredo Mameli: 0000-0001-9175-8965
Bora Karasulu: 0000-0001-8129-8010
Bart Macco: 0000-0003-1197-441X
Adriaan J. M. Mackus: 0000-0001-6944-9867
Wilhelmus M. M. Erwin Kessels: 0000-0002-7630-8226

Author Contributions

All authors have given approval to the final version of the manuscript.

DOI: 10.1021/acs.chemmater.8b03165
Chem. Mater. 2019, 31, 1250−1257

Notes

The authors declare no competing financial interest.

■ ACKNOWLEDGMENTS

The authors would like to thank Cristian van Helvoirt, Jeroen van Gerwen, Tjibbe de Vries, and Janneke Zeebregts for technical assistance. The funding of this research by TNO-Holst Centre (The Netherlands) is gratefully acknowledged. Solliance and the Dutch province of Noord-Brabant are acknowledged for funding the TEM facility.

■ REFERENCES

(1) Fang, M.; Ho, J. C. Area-Selective Atomic Layer Deposition: Conformal Coating, Subnanometer Thickness Control, and Smart Positioning. *ACS Nano* **2015**, *9*, 8651−8654.
(2) Hashemi, F. S. M.; Prasittichai, C.; Bent, S. F. Self-Correcting Process for High Quality Patterning by Atomic Layer Deposition. *ACS Nano* **2015**, *9*, 8710−8717.
(3) Kim, W.-H.; Hashemi, F. S. M.; Mackus, A. J. M.; Singh, J.; Kim, Y.; Bobb-Semple, D.; Fan, Y.; Kaufman-Osborn, T.; Godet, L.; Bent, S. F. A Process for Topographically Selective Deposition on 3D Nanostructures by Ion Implantation. *ACS Nano* **2016**, *10*, 4451−4458.
(4) Mackus, A. J. M.; Bol, A. A.; Kessels, W. M. M. The Use of Atomic Layer Deposition in Advanced Nanopatterning. *Nanoscale* **2014**, *6*, 10941−10960.
(5) Chen, R.; Bent, S. F. Chemistry for Positive Pattern Transfer Using Area-Selective Atomic Layer Deposition. *Adv. Mater.* **2006**, *18*, 1086−1090.
(6) Färm, E.; Lindroos, S.; Ritala, M.; Leskelä, M. Microcontact Printed RuO_x Film as an Activation Layer for Selective-Area Atomic Layer Deposition of Ruthenium. *Chem. Mater.* **2011**, *24*, 275−278.
(7) Mackus, A. J. M.; Mulders, J. J. L.; Van De Sanden, M. C. M.; Kessels, W. M. M. Local Deposition of High-Purity Pt Nanostructures by Combining Electron Beam Induced Deposition and Atomic Layer Deposition. *J. Appl. Phys.* **2010**, *107*, 116102.
(8) Mackus, A. J. M.; Dielissen, S. A. F.; Mulders, J. J. L.; Kessels, W. M. M. Nanopatterning by Direct-Write Atomic Layer Deposition. *Nanoscale* **2012**, *4*, 4477−4480.
(9) Mameli, A.; Kuang, Y.; Aghaee, M.; Ande, C. K.; Karasulu, B.; Creatore, M.; Mackus, A. J. M.; Kessels, W. M. M.; Roozeboom, F. Area-Selective Atomic Layer Deposition of In_2O_3:H Using a μ-Plasma Printer for Local Area Activation. *Chem. Mater.* **2017**, *29*, 921−925.
(10) Kuang, Y.; Macco, B.; Karasulu, B.; Ande, C. K.; Bronsveld, P. C. P.; Verheijen, M. A.; Wu, Y.; Kessels, W. M. M.; Schropp, R. E. I. Towards the Implementation of Atomic Layer Deposition In_2O_3:H in Silicon Heterojunction Solar Cells. *Sol. Energy Mater. Sol. Cells* **2017**, *163*, 43−50.
(11) Sun, K.; Zeimpekis, I.; Hu, C.; Ditshego, N. M. J.; Thomas, O.; de Planque, M. R. R.; Chong, H. M. H.; Morgan, H.; Ashburn, P. Low-Cost Top-down Zinc Oxide Nanowire Sensors through a Highly Transferable Ion Beam Etching for Healthcare Applications. *Microelectron. Eng.* **2016**, *153*, 96−100.
(12) Suresh, V.; Huang, M. S.; Srinivasan, M. P.; Krishnamoorthy, S. In Situ Synthesis of High Density Sub-50 nm ZnO Nanopatterned Arrays Using Diblock Copolymer Templates. *ACS Appl. Mater. Interfaces* **2013**, *5*, 5727−5732.
(13) Bauermann, L.P.; Gerstel, P.; Bill, J.; Walheim, S.; Huang, C.; Pfeifer, J.; Schimmel, T. Templated Self-Assembly of ZnO Films on Monolayer Patterns with Nanoscale Resolution. *Langmuir* **2010**, *26*, 3774−3778.
(14) Chevalier-César, C.; Nomenyo, K.; Rumyantseva, A.; Gokarna, A.; Gwiazda, A.; Lérondel, G. Direct Holographic Patterning of ZnO. *Adv. Funct. Mater.* **2016**, *26*, 1787−1792.
(15) Utke, I.; Hoffmann, P.; Melngailis, J. Gas-Assisted Focused Electron Beam and Ion Beam Processing and Fabrication. *J. Vac. Sci. Technol., B: Microelectron. Nanometer Struct.* **2008**, *26*, 1197−1276.
(16) Jesse, S.; Borisevich, A. Y.; Fowlkes, J. D.; Lupini, A. R.; Rack, P. D.; Unocic, R. R.; Sumpter, B. G.; Kalinin, S. V.; Belianinov, A.; Ovchinnikova, O. S. Directing Matter: Toward Atomic-Scale 3D Nanofabrication. *ACS Nano* **2016**, *10*, 5600−5618.
(17) van Dorp, W. F. Sub-10 Nm Writing: Focused Electron Beam-Induced Deposition in Perspective. *Appl. Phys. A: Mater. Sci. Process.* **2014**, *117*, 1615−1622.
(18) Peinado, P.; Sangiao, S.; De Teresa, J. M. Focused Electron and Ion Beam Induced Deposition on Flexible and Transparent Polycarbonate Substrates. *ACS Nano* **2015**, *9*, 6139−6146.
(19) Wu, Y.; Potts, S. E.; Hermkens, P. M.; Knoops, H. C. M.; Roozeboom, F.; Kessels, W. M. M. Enhanced Doping Efficiency of Al-Doped ZnO by Atomic Layer Deposition Using Dimethylaluminum Isopropoxide as an Alternative Aluminum Precursor. *Chem. Mater.* **2013**, *25*, 4619−4622.
(20) McDonnell, S.; Longo, R. C.; Seitz, O.; Ballard, J. B.; Mordi, G.; Dick, D.; Owen, J. H. G.; Randall, J. N.; Kim, J.; Chabal, Y. J.; et al. Controlling the Atomic Layer Deposition of Titanium Dioxide on Silicon: Dependence on Surface Termination. *J. Phys. Chem. C* **2013**, *117*, 20250−20259.
(21) Melskens, J.; Smets, A. H. M.; Schouten, M.; Eijt, S. W. H.; Schut, H.; Zeman, M. New Insights in the Nanostructure and Defect States of Hydrogenated Amorphous Silicon Obtained by Annealing. *IEEE J. Photovoltaics* **2013**, *3*, 65−71.
(22) Macco, B.; Melskens, J.; Podraza, N. J.; Arts, K.; Pugh, C.; Thomas, O.; Kessels, W. M. M. Correlating the Silicon Surface Passivation to the Nanostructure of Low-Temperature a-Si:H after Rapid Thermal Annealing. *J. Appl. Phys.* **2017**, *122*, 035302.
(23) Blöchl, P. E. Projector Augmented-Wave Method. *Phys. Rev. B: Condens. Matter Mater. Phys.* **1994**, *50*, 17953−17979.
(24) Kresse, G.; Joubert, D. From Ultrasoft Pseudopotentials to the Projector Augmented-Wave Method. *Phys. Rev. B: Condens. Matter Mater. Phys.* **1999**, *59*, 1758−1775.
(25) Kresse, G.; Hafner, J. *Ab Initio* Molecular Dynamics for Liquid Metals. *Phys. Rev. B: Condens. Matter Mater. Phys.* **1993**, *47*, 558−561.
(26) Kresse, G.; Hafner, J. *Ab Initio* Molecular-Dynamics Simulation of the Liquid-Metal−amorphous-Semiconductor Transition in Germanium. *Phys. Rev. B: Condens. Matter Mater. Phys.* **1994**, *49*, 14251−14269.
(27) Kresse, G.; Furthmüller, J. Efficiency of *Ab-Initio* Total Energy Calculations for Metals and Semiconductors Using a Plane-Wave Basis Set. *Comput. Mater. Sci.* **1996**, *6*, 15−50.
(28) Hohenberg, P.; Kohn, W. Inhomogeneous Electron Gas. *Phys. Rev.* **1964**, *136*, B864−B871.
(29) Kohn, W.; Sham, L. J. Self-Consistent Equations Including Exchange and Correlation Effects. *Phys. Rev.* **1965**, *140*, A1133−A1138.
(30) Perdew, J. P.; Burke, K.; Ernzerhof, M. Generalized Gradient Approximation Made Simple. *Phys. Rev. Lett.* **1997**, *78*, 1396.
(31) Grimme, S.; Antony, J.; Ehrlich, S.; Krieg, H. A Consistent and Accurate Ab Initio Parametrization of Density Functional Dispersion Correction (DFT-D) for the 94 Elements H-Pu. *J. Chem. Phys.* **2010**, *132*, 154104.
(32) Mameli, A.; Merkx, M. J. M.; Karasulu, B.; Roozeboom, F.; Kessels, W. M. M.; Mackus, A. J. M. Area-Selective Atomic Layer Deposition of SiO_2 Using Acetylacetone as a Chemoselective Inhibitor in an ABC-Type Cycle. *ACS Nano* **2017**, *11*, 9303−9311.
(33) Henkelman, G.; Uberuaga, B. P.; Jónsson, H. A Climbing Image Nudged Elastic Band Method for Finding Saddle Points and Minimum Energy Paths. *J. Chem. Phys.* **2000**, *113*, 9901.
(34) VTST Tool Set for VASP.
(35) Puurunen, R. L.; Vandervorst, W. Island Growth as a Growth Mode in Atomic Layer Deposition: A Phenomenological Model. *J. Appl. Phys.* **2004**, *96*, 7686−7695.
(36) Michalak, D. J.; Amy, S. R.; Aureau, D.; Dai, M.; Estève, A.; Chabal, Y. J. Nanopatterning Si(111) surfaces as a selective surface-chemistry route. *Nat. Mater.* **2010**, *9*, 266−271.
(37) Kramer, N.; Jorritsma, J.; Birk, H.; Schönenberger, C. Nanometer Lithography on Silicon and Hydrogenated Amorphous-Silicon with Low-Energy Electrons. *Microelectron. Eng.* **1995**, *27*, 47−50.
(38) Ikeda, H.; Hotta, K.; Yamada, T.; Zaima, S.; Iwano, H.; Yasuda, Y. Oxidation of H-Terminated Si(100) Surfaces Studied by High-

DOI: 10.1021/acs.chemmater.8b03165
Chem. Mater. 2019, 31, 1250−1257

Resolution Electron Energy Loss Spectroscopy. *J. Appl. Phys.* **1995**, *77*, 5125−5129.
(39) Gladfelter, W. L. Selective Metallization by Chemical-Vapor-Deposition. *Chem. Mater.* **1993**, *5*, 1372−1388.
(40) Sánchez, E. J.; Krug, J. T.; Xie, X. S. Ion and Electron Beam Assisted Growth of Nanometric SimOn Structures for near-Field Microscopy. *Rev. Sci. Instrum.* **2002**, *73*, 3901.
(41) Frabboni, S.; Gazzadi, G. C.; Spessot, A. Transmission Electron Microscopy Characterization and Sculpting of Sub-1 Nm Si-O-C Freestanding Nanowires Grown by Electron Beam Induced Deposition. *Appl. Phys. Lett.* **2006**, *89*, 112108.
(42) Perentes, A.; Hoffmann, P. Oxygen Assisted Focused Electron Beam Induced Deposition of Si-Containing Materials: Growth Dynamics. *J. Vac. Sci. Technol., B: Microelectron. Nanometer Struct.* **2007**, *25*, 2233−2238.
(43) Aria, A. I.; Nakanishi, K.; Xiao, L.; Braeuninger-Weimer, P.; Sagade, A. A.; Alexander-Webber, J. A.; Hofmann, S. Parameter Space of Atomic Layer Deposition of Ultrathin Oxides on Graphene. *ACS Appl. Mater. Interfaces* **2016**, *8*, 30564−30575.
(44) Seo, S.; Yeo, B. C.; Han, S. S.; Yoon, C. M.; Yang, J. Y.; Yoon, J.; Yoo, C.; Kim, H.-j.; Lee, Y.-b.; Lee, S. J.; Myoung, J.-M.; Lee, H.-B. -R.; Kim, W.-H.; Kim, H.; Oh, I.-K.; Kim, H. Reaction Mechanism of Area-Selective Atomic Layer Deposition for Al_2O_3 Nanopatterns. *ACS Appl. Mater. Interfaces* **2017**, *9*, 41607−41617.

DOI: 10.1021/acs.chemmater.8b03165
Chem. Mater. 2019, 31, 1250−1257